SFT VOL. 68 ISSUE 2, 2026, PP. 48–60

Cédric Tiafoudji, El-Kebir Iya Ahmed, Ruben Mouangue

National Higher Polytechnic School of Douala, Laboratory of Energy, University of Douala

Philippe Onguene Mvogo

School of Chemical Engineering and Mineral Industries, University of Ngaoundéré

Fidel Meskéoulé Vondou

Faculty of Science, University of Garoua

Justin Tégawendé Zaida

Higher Polytechnic School of Ouagadougou, University of Ouagadougou

Corresponding author: philippe.onguene@egcim-univ-ndere.com

Modelling of the Dispersion of Butane in an Enclosed Space on the Example of a Professional Kitchen

Modelowanie rozprzestrzeniania się butanu w przestrzeni zamkniętej na przykładzie kuchni gastronomicznej

ABSTRACT

Purpose: This study investigates the dispersion of liquefied petroleum gas (LPG) following an accidental leak in an unoccupied commercial kitchen, with the objective of identifying areas with critical gas concentration levels that may lead to fire or explosion if an ignition source is introduced. Understanding the spatial and temporal evolution of leaked gas is essential for improving fire prevention strategies, optimizing ventilation design, and enhancing the safety of commercial cooking environments.

Project and methods: A three-dimensional Computational Fluid Dynamics (CFD) model was developed to simulate the release and dispersion of gas inside a closed kitchen enclosure measuring 2 × 2 × 2 m. A realistic leak source was characterized by a constant mass flow rate of 0.3611 g/s under quiescent conditions. The numerical model enabled the prediction of gas concentration fields, flow structures, turbulence intensity, and Reynolds number distribution throughout the transient leakage process. Particular attention was paid to the evolution of combustible gas accumulation and to the identification of regions where flammable mixtures are likely to develop.

Results: The simulation results reveal that the highest gas concentrations accumulate and stabilize approximately 10 cm above the floor, confirming the tendency of leaked gas to remain in the lower part of the enclosure. The flow is characterized by significant turbulence in the vicinity of the leakage source, where the Reynolds number reaches a maximum value of 23 597, promoting rapid mixing between the leaked gas and the surrounding air. In contrast, gas concentrations remain negligible at heights exceeding 1 m during the transient phase, indicating that the upper part of the kitchen remains essentially unaffected throughout the leakage period.

Conclusions: These findings demonstrate that areas with critical concentration levels are located near the floor, where combustible mixtures are more likely to persist and where ignition sources would present the greatest risk of fire and explosion. The study provides valuable insights into the behaviour of accidental gas leaks in confined commercial kitchens and contributes to the development of safer kitchen layouts, improved ventilation strategies, and more effective fire risk assessment methodologies.

Keywords: OpenFOAM, simulation, confined fire, critical concentration

Type of article: original scientific article

Received: 20.07.2026; Reviewed: 14.09.2026; Accepted: 06.10.2026;
Authors' ORCID IDs: C. Tiafoudji – 0009-0000-3334-8888; El-K. I. Ahmed – 0009-0004-3585-7546; R. Mouangue – 0000-0003-2454-3088; Ph. O. Mvogo – 0000-0002-4542-5390; F. M. Vondou – 0009-0009-8080-0158; J. T. Zaida – 0000-0002-0008-0704
The authors contributed equally to this article;
Please cite as: Safety & Fire Technology 2026, 2, 48–60, https://doi.org/10.12845/sft.68.2.2026.3;
This is an open access article under the CC BY-SA 4.0 license (https://creativecommons.org/licenses/by-sa/4.0/).

ABSTRAKT

Cel: Celem pracy była analiza rozprzestrzeniania się gazu płynnego (LPG) wskutek przypadkowego wycieku w kuchni gastronomicznej oraz wskazanie miejsc, w których stężenie gazu może stwarzać zagrożenie pożarem lub wybuchem w przypadku pojawienia się źródła zapłonu. W analizowanym scenariuszu przyjęto, że w czasie wycieku w pomieszczeniu nie przebywają ludzie. Określenie zmian stężenia uwolnionego gazu w czasie i przestrzeni ma istotne znaczenie dla zapobiegania pożarom, właściwego projektowania wentylacji oraz poprawy bezpieczeństwa w kuchniach gastronomicznych.
Projekt i metody: Opracowano trójwymiarowy model z wykorzystaniem obliczeniowej mechaniki płynów (CFD), umożliwiający symulację uwalniania i rozprzestrzeniania się gazu w zamkniętym pomieszczeniu o wymiarach 2 × 2 × 2 m. Źródło wycieku odwzorowano, przyjmując stałe masowe natężenie wypływu wynoszące 0,3611 g/s oraz brak początkowego ruchu powietrza. Model numeryczny pozwolił określić rozkład stężenia gazu, strukturę przepływu, intensywność turbulencji oraz rozkład liczby Reynoldsa podczas wycieku. Szczególną uwagę poświęcono gromadzeniu się gazu palnego oraz określeniu miejsc, w których mogą powstawać mieszaniny palne.
Wyniki: Wyniki symulacji wskazują, że największe stężenie gazu występuje i stabilizuje się na wysokości około 10 cm nad podłogą. Potwierdza to tendencję gazu do gromadzenia się w dolnej części pomieszczenia. W pobliżu źródła wycieku przepływ charakteryzuje się znaczną turbulencją. Liczba Reynoldsa osiąga w tym obszarze maksymalną wartość 23 597, co sprzyja szybkiemu mieszaniu się uwolnionego gazu z otaczającym powietrzem. Na wysokości powyżej 1 m stężenie gazu w analizowanym okresie pozostaje natomiast znikome. Oznacza to, że wyciek praktycznie nie wpływa na warunki panujące w górnej części pomieszczenia.
Wnioski: Wyniki wskazują, że miejsca, w których stężenie gazu osiąga wartości krytyczne, znajdują się w pobliżu podłogi. W tej części pomieszczenia mieszaniny palne mogą utrzymywać się najdłużej, a obecność źródła zapłonu stwarza największe zagrożenie pożarem lub wybuchem. Badanie dostarcza istotnych informacji na temat przebiegu przypadkowych wycieków gazu w zamkniętych kuchniach gastronomicznych oraz może wspierać projektowanie bezpieczniejszych pomieszczeń, doskonalenie rozwiązań wentylacyjnych i rozwój skuteczniejszych metod oceny ryzyka pożarowego.
Słowa kluczowe: OpenFOAM, symulacja, pożar zamknięty, stężenie krytyczne
Typ artykułu: oryginalny artykuł naukowy

Przyjęty: 20.07.2026; Zrecenzowany: 14.09.2026; Zaakceptowany: 06.10.2026;
Identyfikatory ORCID autorów: C. Tiafoudji – 0009-0000-3334-8888; El-K. I. Ahmed – 0009-0004-3585-7546; R. Mouangue – 0000-0003-2454-3088; Ph. O. Mvogo – 0000-0002-4542-5390; F. M. Vondou – 0009-0009-8080-0158; J. T. Zaida – 0000-0002-0008-0704
Autorzy wnieśli równy wkład merytoryczny w opracowanie artykułu;
Proszę cytować: Safety & Fire Technology 2026, 2, 48–60, https://doi.org/10.12845/sft.68.2.2026.3;
Artykuł udostępniany na licencji CC BY-SA 4.0 (https://creativecommons.org/licenses/by-sa/4.0/).

Introduction

The build-up of gas in enclosed spaces is a major safety concern [1], particularly when it comes to flammable or explosive gases. Commercial kitchens and unattended cooking are the leading causes of fires in the United States [2], and represent environments where the risks of gas accumulation are heightened due to the concentration of heat-generating equipment, potential gas leaks and the use of fuels. Studying the critical gas concentration in these enclosed spaces is essential for preventing accidents, whether these involve explosions, fires or poisoning from gases such as methane, butane or propane. In this context, modelling the accumulation and concentration of gases within an enclosed space, such as a commercial kitchen, is essential for assessing and preventing potential risks. The concept of 'critical gas concentration' refers to the minimum concentration of gas in an enclosed space at which the probability of an explosion or fire becomes significant, based on the lower and upper explosive limits (LEL and UEL). Inadequate or poorly designed ventilation can quickly lead to concentration levels exceeding critical thresholds [3]. Furthermore, these environments present a context in which safety issues are particularly sensitive, as an explosion could result in loss of life [4]. As the flash point is a very important characteristic of any fluid, it can significantly affect the combustion regime, which may lead to a rapid explosion or, in critical cases within tunnels, develop into a detonation [5]. Certain materials are sometimes found to have a dominant influence on gas diffusion behaviour, which can be observed using a new pressure-based diffusion coefficient model [6]. Several test gases have already been evaluated, visualised and validated in the field of gas dispersion in closed chambers, such as helium [7], hydrogen [8] and chlorine [9].

Aims

Using a numerical approach that optimises computational costs while analysing key fields for more accurate assessment of the risk of explosion, this study models the dispersion of butane

in an air-filled enclosed space, investigates the influence of fluid dynamics, and analyses high-risk areas to identify zones with critical gas concentrations as shown in Figure 1.

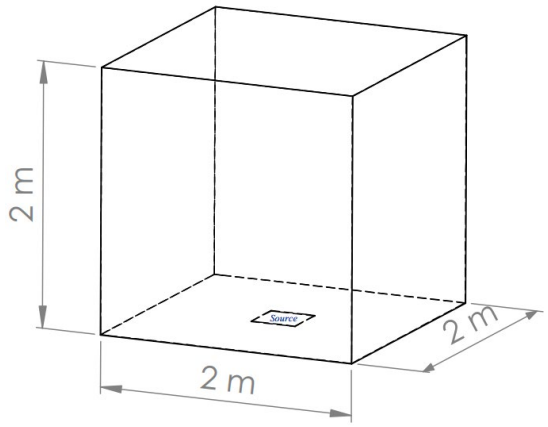


Figure 1. Kitchen enclosure under consideration (2 x 2 x 2 m). 'Source' is shown in blue in the centre

Source: Own elaboration.

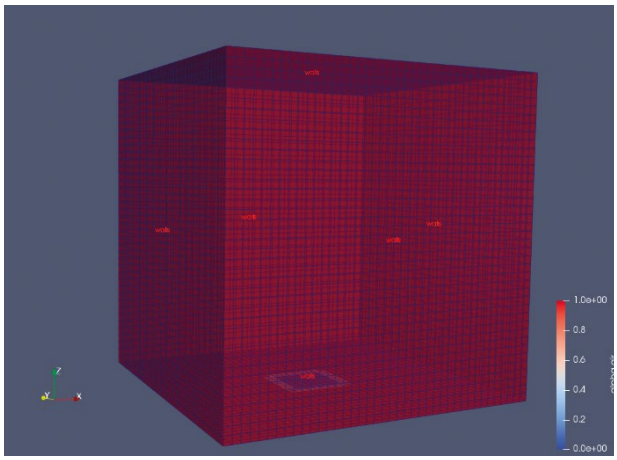


Figure 2. Kitchen enclosure mesh (2 x 2 x 2 m). 'Wall' is marked in red on each wall

Source: Own elaboration.

The CFD simulations associated with this work are validated using several established numerical methods, including codes such as CFD Fluent [9], CFD-FLACS [10], CFD Flacs Hydrogen [11], ANSYS [12], FDS [13], [14] and OpenFOAM [15].

Materials and Methods

Numerical Code

One of the most important CFD software packages in recent years is OpenFOAM (Open Field Operation and Manipulation). In a single package, it brings together a large library of interconnected applications capable of solving a vast array of scientific problems. OpenFOAM is an open-source computational fluid dynamics simulation software package created by Weller et al. (1998) [16]. He began developing the software, then known as 'FOAM', in 1989. Henry Weller, the lead developer of this software, is also a co-founder of the OpenFOAM Foundation, established in the United States on 5 August 2011, which distributes OpenFOAM under an open-source licence.

Regarded as the primary visualisation tool provided with OpenFOAM, ParaView enables the analysis and visualisation of CFD simulation results produced using OpenFOAM. There is also an older viewer for OpenFOAM called paraFoam, but ParaView is more effective at visualising OpenFOAM data and is a registered trademark of Kitware [17].

This application enabled us to explore, analyse and present the fields calculated in this work, such as the air volume fraction, the turbulent kinetic energy dissipation rate, the turbulent kinetic energy, the turbulent kinematic viscosity, the static pressure, the hydrostatic pressure, and the fluid velocity. The meshing was carried out using 'blockMesh', the modelling and simulation using 'OpenFOAM-6', and the results were analysed in 'ParaView' (see Figure 3). To ensure the numerical calculations ran smoothly and with good stability, a Dell Latitude 5500 was selected, featuring an 8th-generation Core i7 processor, 512 GB SSD storage, 32 GB RAM, 8 CPUs, an integrated Intel UHD Graphics 620 graphics card with 16 GB of memory, a 15.6-inch screen and a 64-bit Ubuntu 18.04 (Linux) operating system.

Professional Kitchen and Gas Model

A professional kitchen, such as in a hotel, is not a conventional kitchen, as it is subject to specific health and safety regulations [18] imposed by various international standards. This purpose-built space is designed specifically for the preparation of large quantities of food in accordance with precise standards [19]. For the purposes of this study, the authors use as a model the kitchen of a local cement factory, the dimensions of which have been scaled down. It is located in the port industrial zone of Douala, with butane as the cooking gas. The properties of the gas and air within the enclosure are shown in Table 1.

Butane is an alkane, a type of saturated hydrocarbon whose molecular composition consists of carbon (C) and hydrogen (H) atoms. Its chemical formula is C_4H_{10}; it can be liquefied under pressure at room temperature and stored in cylinders or tanks. Pure butane is colourless and odourless; for safety reasons, a small amount of an odorant is added to it so that leaks can be easily detected in an enclosed space. Butane is a Liquefied Petroleum Gas (LPG) extracted in small quantities from natural gas and in large quantities from crude oil during refining.

Mathematical model

The RNG *k-ε* model (Yakhot et al., 1986) [20] incorporates corrections derived from renormalisation group theory. It improves the representation of high-shear flows and separations, whilst providing a better fit for turbulent viscosity. The RNG *k-ε* model derives from a rigorous statistical technique known as 'Renormalisation Group' theory. It is similar to the standard *k-ε* model but includes certain improvements. Of the available turbulence models, the RNG *k-ε* model has been selected for this study.

This choice is justified by the fact that, having been developed using group renormalisation theory (RNG), it provides an

analytical formulation of the constants, making it more general and accurate than its standard counterpart, the Reynolds-averaged Navier-Stokes (RANS) equations. It is particularly well-suited to shear flows with steep velocity gradients, which are typical of gas jets. The study examines the dispersion of gaseous butane within a closed chamber, with the aim of determining the critical concentration likely to reach or exceed a safety threshold governed by the LEL and UEL. This phenomenon is transient and involves a difference in density compared to air, resulting in buoyancy and stratification effects. The carrier fluid is air, which is considered incompressible, with gas dispersion governed by convection due to air flows and by diffusion. All these flow characteristics have guided our choice not only of a turbulence model, but also of a model that takes into account a large part of the characteristics of our flow, including buoyancy and the turbulent Reynolds number of the gas leak in question. This model is implemented and parameterized according to its structure in the OpenFOAM computational code and coupled with the interFoam solver; it has been numerically verified and qualitatively compared with the results of several studies in the same scientific context [21], [22]; direct experimental validation has yet to be carried out [23]. The equations solved in this code are based on the principles of conservation of mass, momentum, chemical species and turbulence:

(a) Conservation of mass:

$$\iiint_{V(t)} \left(\frac{\partial \rho}{\partial t} + \nabla \cdot (\rho u) \right) dV = 0 \tag{1}$$

(b) Conservation of momentum:

$$\iiint_{V(t)} \left(\frac{\partial (\rho u)}{\partial t} + \nabla \cdot (\rho u \otimes u) \right) dV = \iiint_{V(t)} (\rho f + \nabla \cdot T) dV \tag{2}$$

(c) Conservation of energy:

$$\iiint_{V(t)} \left(\frac{\partial (\rho e_{tot})}{\partial t} + \nabla \cdot (\rho e_{tot} u) \right) dV = \iiint_{V(t)} (- \nabla \cdot q + \rho s + \nabla \cdot (T \cdot u)) dV \tag{3}$$

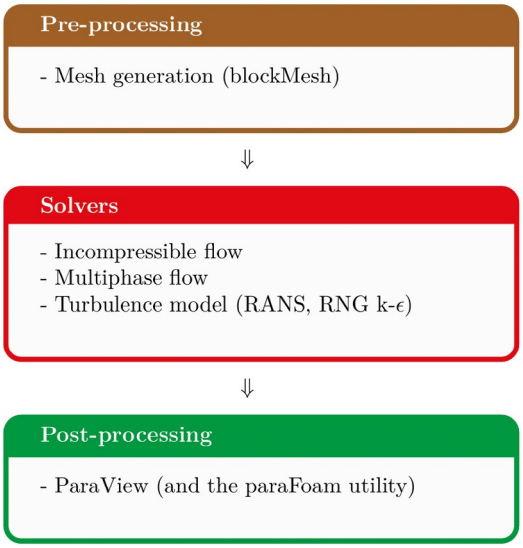


Figure 3. Calculation launch process

Source: Own elaboration.

A total of seven fields were calculated in this study:

- The volume fraction of air (a_{air} or *alpha.air*)
- The turbulent kinetic energy dissipation rate (ε)
- The turbulent kinetic energy (k)
- The turbulent kinematic viscosity (v_t or *nut*)
- The static pressure (p)
- The hydrostatic pressure (p_rgh)
- The fluid velocity (U)

Table 1. Air and butane properties

Air	Butane
$\rho_{air} = 1.204\ kg \cdot m^{-3}$	$\rho_{but} = 2.52\ kg \cdot m^{-3}$
$v_{air} = 1.562 \cdot 10^{-5} m^2 \cdot s^{-1}$	$v_{but} = 2.77 \cdot 10^{-6} m^2 \cdot s^{-1}$
$\mu_{air} = 1.88 \cdot 10^{-5} kg \cdot m^{-1} \cdot s^{-1}$	$\mu_{but} = 7 \cdot 10^{-6} kg \cdot m^{-1} \cdot s^{-1}$
-	LEL: 1.8%
-	UEL: 8.4%

Source: Own elaboration.

(d) Equation for turbulent kinetic energy:

$$\frac{\partial (\rho k)}{\partial t} + \nabla \cdot (\rho U k) = \nabla \cdot \left[\left(\mu + \frac{\mu_t}{\sigma_k} \right) \nabla k \right] + \rho G - \rho \epsilon - \frac{2}{3} \rho k \nabla \cdot U \tag{4}$$

(e) Dissipation equation:

$$\frac{\partial (\rho \epsilon)}{\partial t} + \nabla \cdot (\rho U \epsilon) = \nabla \cdot \left[\left(\mu + \frac{\mu_t}{\sigma_\epsilon} \right) \nabla \epsilon \right] +$$
$$+ (C_1 - R) \frac{\rho \epsilon}{k} G - C_2 \rho \frac{\epsilon^2}{k} - \left(\frac{2}{3} C_1 - C_3 \right) \rho \epsilon \nabla \cdot U \tag{5}$$

(f) Equation for turbulent kinematic viscosity:

$$v_t = C_\mu \frac{k^2}{\epsilon} \tag{6}$$

(g) Correction factor equation:

$$R(\eta) = \frac{\eta (1 - \eta / \eta_0)}{1 + \beta \eta^3} \tag{7}$$

with

$$\eta = \frac{\sqrt{S_{ij} S_{ij}}\, k}{\epsilon} \tag{8}$$

where S_{ij} is the strain tensor.

(h) The model coefficients are [17]:

- $C_\mu = 0.0845$;
- $C_1 = 1.42$;
- $C_2 = 1.68$;
- $C_3 = 0$;
- $\sigma_k = 0.71942$;
- $\sigma_\varepsilon = 0.71942$;
- $\eta_0 = 4.38$;
- $\beta = 0.012$.

(i) The effective diffusivities:

$$D_k^{eff} = \nu + \frac{\nu_t}{\sigma_k} \qquad D_\epsilon^{eff} = \nu + \frac{\nu_t}{\sigma_\epsilon} \tag{9}$$

The ability of gas to diffuse is characterised by diffusivities. This parameter describes the rate at which fluids propagate and mix. In the examined case, the expressions for the diffusivities of turbulent kinetic energy (k) and dissipation (ε) are given in Equation 9 of this article. This equation depends on the molecular kinematic viscosity, the turbulent kinematic viscosity, and the turbulent Prandtl numbers of k and ε. Given the often mixed nature of fluids, the weighted average kinematic viscosity (v_{weig}) is defined [24], [25] by the following equation :

$$\nu_{weig} = \frac{\alpha_{air} \cdot \mu_{air} + (1-\alpha_{air})\mu_{but}}{\alpha_{air} \cdot \rho_{air} + (1-\alpha_{air})\rho_{but}} \tag{10}$$

With this new formulation of the weighted kinematic viscosity, Equation 9 for the effective diffusivities becomes:

$$D_k^{eff} = \nu_{weig} + \frac{\nu_t}{\sigma_k} \qquad D_\epsilon^{eff} = \nu_{weig} + \frac{\nu_t}{\sigma_\epsilon} \tag{11}$$

Mesh of the enclosed enclosure

The numerical model used for the study was created with dimensions of 2 × 2 × 2 m, giving a volume of 8 m^3. The mesh was generated with 68,921 nodes, 196,800 faces, 187 200 internal faces, and 64 000 cubic cells of dimensions (0.05 × 0.05 × 0.05 m) at a rate of 40 on each side. The results of the calculations are analysed using images and curves at different time intervals. The analysis is carried out at different critical times, with lines on the horizontal (diagonal) and vertical (lateral) planes. Each field is first analysed separately and then as a group. When the mesh grid is hidden, the following result is obtained in Figure 4 below.

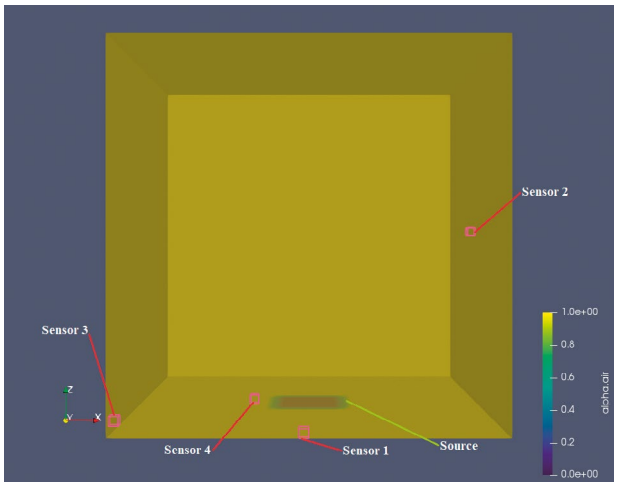


Figure 5. Source and virtual measurement points within the enclosure. The legend ranges from 0(0%) to 1(100%)

Source: Own elaboration.

The kitchen enclosure is modelled according to the following principle: a gas box positioned at (0.8, 0.8, 0.0) within the enclosure, at its base, representing the kitchen floor. This box, with numerical dimensions of (1.2 × 1.2 × 0.1 m for the LEL and 1.2 x 1.2 x 0.467 for the UEL), is coloured blue (Figure 2) or green (Figure 4) and is completely filled (100%) with butane gas of initial density (2.52 kg · m^{-3}). The kitchen enclosure is initially filled with 8 m^3 of air (100%), shown in red (Figure 2) or yellow olive (Figure 4), with an initial density of (1.204 kg · m^{-3}). The enclosure is completely sealed, hence the absence of windows and doors. These doors also constitute a major simulation parameter in several studies on fire safety [26], [27].

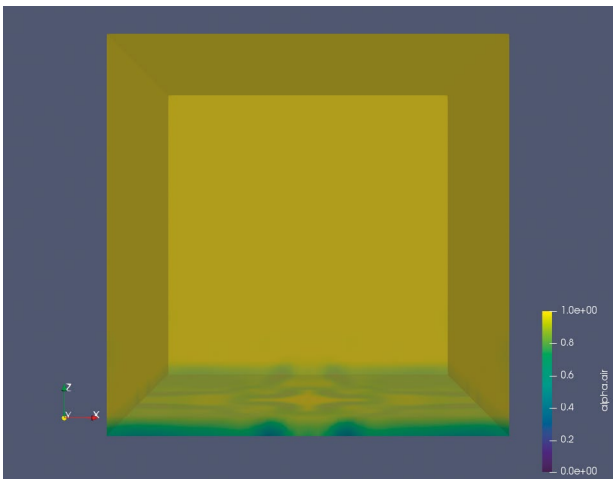
Results and Discussion

Visual and graphical dynamics of LEL fields

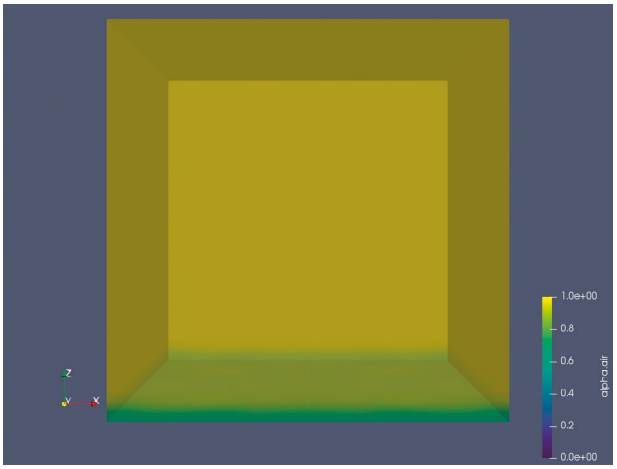
The gas canister placed inside the chamber and initially completely filled has a volume of 0.144 m^3, representing 1.8% of the chamber, as shown in Figure 4. When the gas is released, it gradually spreads throughout the chamber. Using the LEL critical value, the distribution of the gas within the chamber can be analysed. The graphical fields are analysed in detail at different positions. The chamber measures 2 × 2 × 2 m with a diagonal extending from one corner to another. The diagonal is estimated to have a length of $\sqrt{2^2+2^2} = \sqrt{8}\,m$; the approximate length of the diagonal of this cube is $< \sqrt{8}\,m \approx 2.83\,m >$. This diagonal will be used to accurately visualise the effects of the propagation and proportions of the various fields analysed in this study. Another line on the side face will allow us to compare the differences observed between the centre and the areas near the walls.

The volume fraction of air and butane (LEL)

Figure 5 below shows the distribution of butane and air concentrations within the chamber; the image on the left was captured after 5 seconds and the one on the right after 10 seconds. This result demonstrates the high concentration of gas in the lower part of the enclosure:



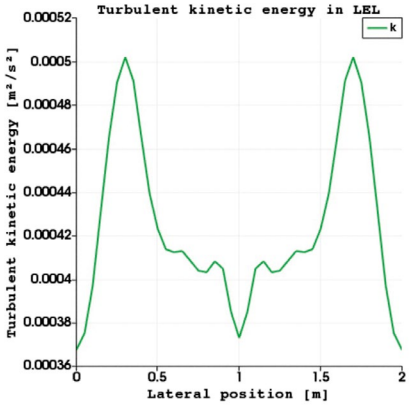
a)



b)

Figure 5. Distribution of air (and butane) within the enclosure at 5 s (a) and 10 s (b). The legend for alpha.air and alpha.butane ranges from 0(0%) to 1(100%)

Source: Own elaboration.



b)

Figure 6. Turbulent kinetic energy at a height of 0.05 m at 10 s: a) diagonal position b) lateral position

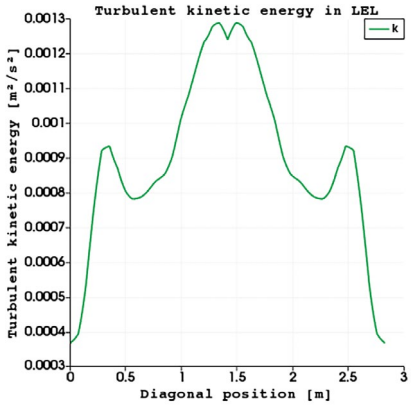
Source: Own elaboration.

The butane is concentrated towards the bottom of the chamber because the chamber was initially filled with air. This air therefore makes way for the butane gas, which initially swirls and then stabilises almost completely near the floor from 10 seconds onwards. It should be noted that this is close to reality as the density of butane gas is greater than that of air. Areas close to the ground present a high risk of explosion should a source of ignition be present.

Geometry of turbulent kinetic energy (LEL)

Within the kitchen enclosure, the energy varies, ranging from low values near the walls and gradually increasing towards the centre of the enclosure before gradually decreasing back to the level of the walls. Looking at the variations in the peaks in Figure 6, it becomes clear that the area dominated by high values of turbulent kinetic energy is the centre of the chamber in the diagonal direction. The lateral direction of the chamber is dominated instead by very low values at the centre and also at approximately 0.25 m in length, with a peak of over 0.0005 m^2/s^2. Nevertheless, a slight correlation of low values is observed across all areas close to the chamber walls.

Figure 6 below shows two images highlighting the critical points of turbulent kinetic energy.

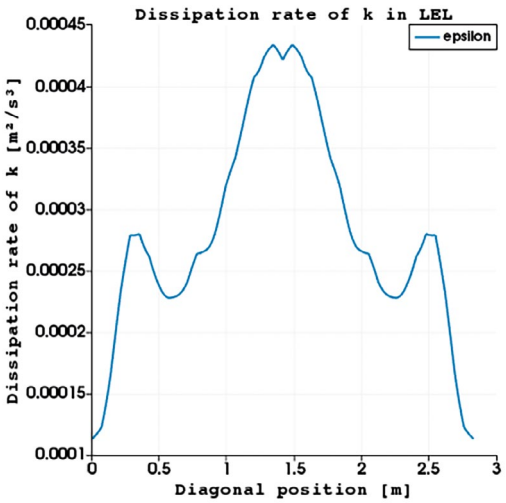


a)

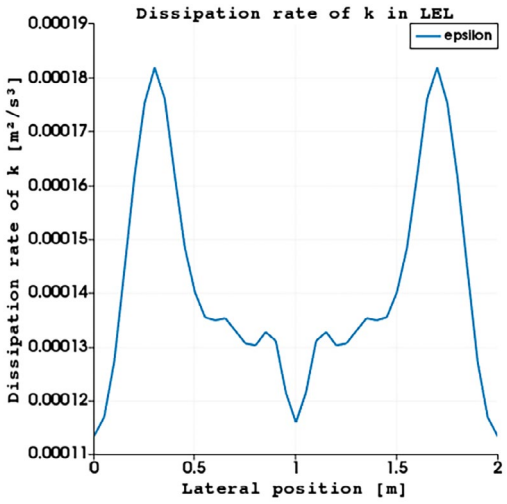
The distribution of *k* indicates areas where air-butane concentrations change rapidly and is indirectly linked to these concentrations for the assessment of the formation of flammable atmosphere; this applies to areas close to the ground around the source.

Geometry of the k-dissipation rate (LEL)

The dissipation-rate field, ε , complements k's analysis of dispersion mechanisms. The shape of the curve showing the evolution of the dissipation rate is almost identical to that of the turbulent energy, albeit with different values. However, a general overview is provided by the graphical representation of this field in the Figure 7 below.



a)



b)

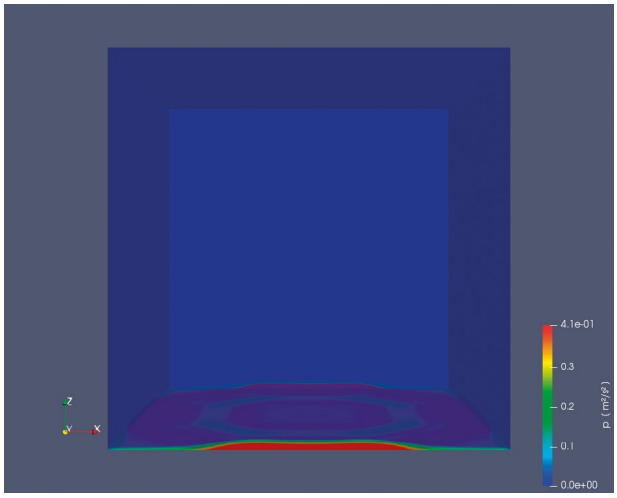
Figure 7. The dissipation rate of k at a height of 0.05 m at 10 s: a) diagonal, b) lateral position

Source: Own elaboration.

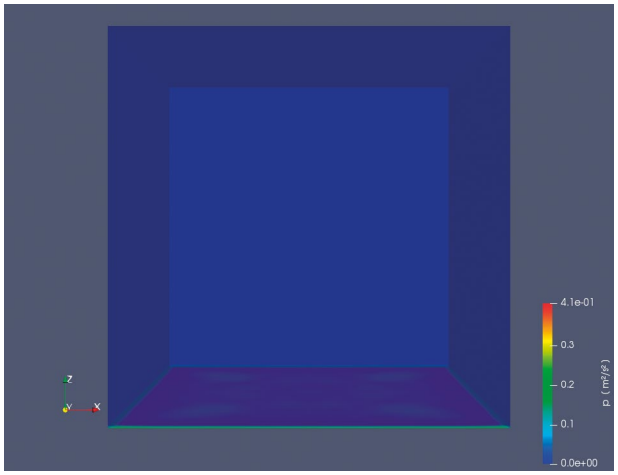
This graph was captured at the tenth minute, and the same applies to the k-field. The peaks are divided into three: the largest, of approximately 0.00045 m^2/s^3, is at the centre of the chamber; the average peak, around 0.00025 m^2/s^3, is at 0.05m diagonally; and the weakest peak, close to 0.0001 m^2/s^3, is near the walls. As for the diagram on the right showing the lateral values, the highest peak is close to 0.00018 m^2/s^3 at approximately 0.25 m along the lateral length, with a low value at the centre of the walls, namely around 0.00012 m^2/s^3.

Static pressure (LEL)

The analysis of this field is required to ensure the consistency of the numerical model and is not directly related to the risk of explosion, but rather to the state and motion of the gas mixture, as shown in Figure 8. The one on the left was taken at 1.5 s, and the one on the right at 10 s. Very violent effects are observed at ground level initially, and then the situation stabilises almost completely towards the bottom of the chamber after a relatively long time.



a)



b)

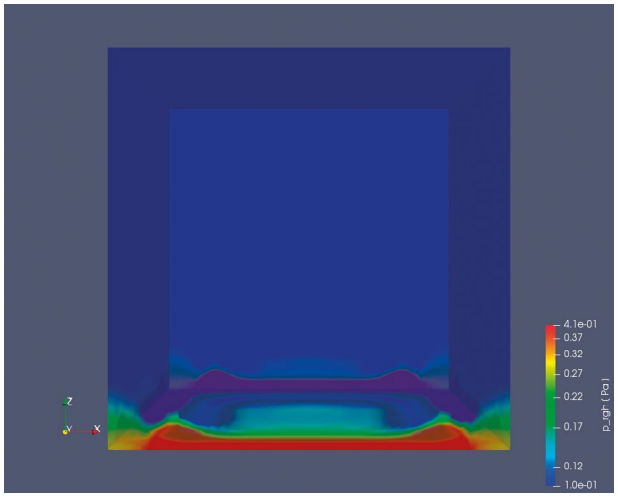
Figure 8. Effect of pressure (kinematic static pressure) in the enclosure at 1.5 s (a) and 10 s (b). The legend for p ranges from 0 m^2/s^2 to 4.1 x 10^{-1} m^2/s^2, this pressure was obtained by division using a local p

Source: Own elaboration.

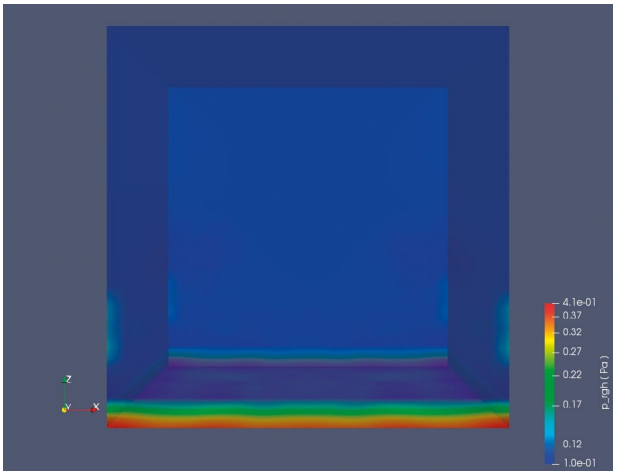
The lower part of the chamber is dominated by very high readings in red; this is practically at ground level, and this rise is observed as soon as the butane gas is released into the chamber. It then moves towards the corners, before returning towards the centre and stabilising at almost 1 cm from the ground from the tenth second of dissipation. This parameter is used to characterise the pressure conditions of the mixture of fluids within the chamber and, where applicable, any changes in pressure at a specific location.

Hydrostatic pressure (LEL)

This other pressure reflects the effect of the weight of the fluids at the bottom of the chamber, stabilising more or less throughout the chamber. It is also a parameter that depends on the depth of the chamber, the density of the fluid and gravity. For this pressure, we observe significant turbulence initially as the butane begins to spread throughout the chamber, followed by stability towards the bottom and slightly in the corners. Figure 9 below illustrates the effects of hydrostatic pressure within the enclosure.



a)



b)

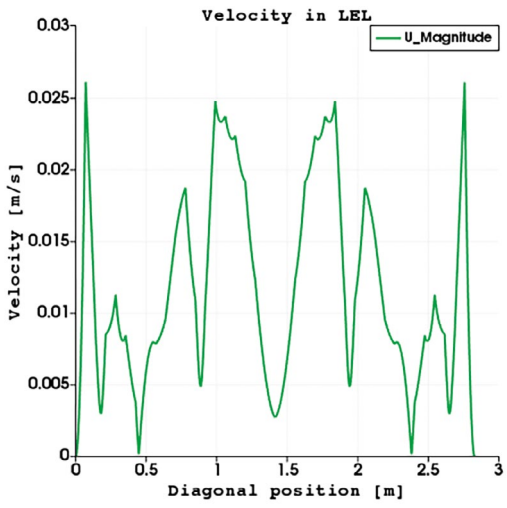
Figure 9. Effect of hydrostatic pressure (pseudo-hydrostatic pressure) in the enclosure at 2 s and 10 s. The legend for $p_{_rgh}$ ranges from 1.0 x 10^{-1} Pa to 4.1 x 10^{-1} Pa

Source: Own elaboration.

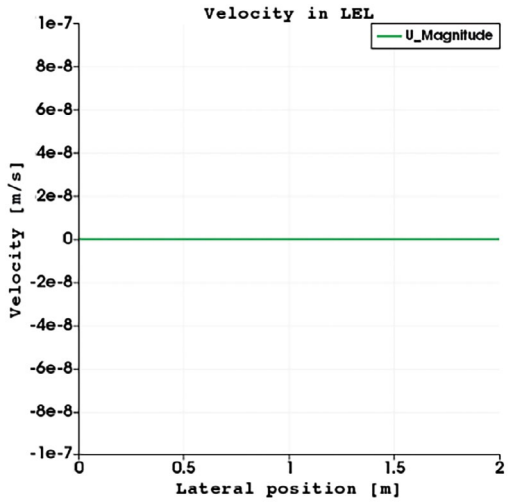
The second is marked by a turbulent disturbance at the bottom of the chamber, which gradually settles down at the bottom. The variations in height remain within a relatively narrow range. p_rgh solves the problem of gravity-driven flow.

Geometry of the propagation velocity (LEL)

The velocity vector field with which the gas spreads through the chamber at the tenth second is relatively weak and stable. Its graphical variations, symmetrical with respect to the chamber, highlight very high peaks and very low troughs. The image on the left was taken diagonally across the chamber, and the one on the right was taken laterally, close to the kitchen walls. In this scenario, these two images captured at identical times clearly show that one cannot rely on a single trajectory to analyse the behaviour of the velocity within the kitchen enclosure:



a)



b)

Figure 10. The propagation velocity at a height of 0.05 *m* at 10 *s*: a) diagonal, b) lateral position

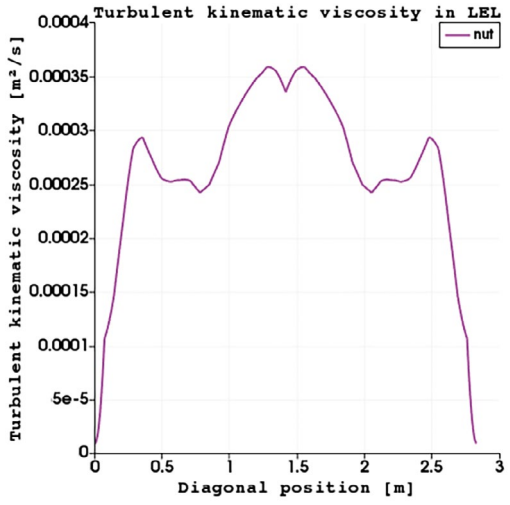
Source: Own elaboration.

Figure 10 above shows two graphs: one with a peak instability and the other, on the right, which is almost linear. The graph on the left has a high peak of approximately 0.026 m/s and a low peak of 0 m/s. The propagation velocity is therefore zero near the walls and then rises abruptly as one begins to move away from the walls, followed by an irregular decrease to a value of approximately 0.003 m/s at the centre of the chamber. Variation in velocity facilitate the transport and mixing of butane; the extent of the explosion-hazard zones therefore depends on the speed of propagation.

Geometry of turbulent kinematic viscosity (LEL)

The turbulent kinematic viscosity is also closely related to the curvatures of k and ε, as these values are all governed by the same basic formulation (Equation 6).

Figure 11 below shows the variation of v_t at a height of 0.05 m for the diagonal direction and for the lateral direction.



a)

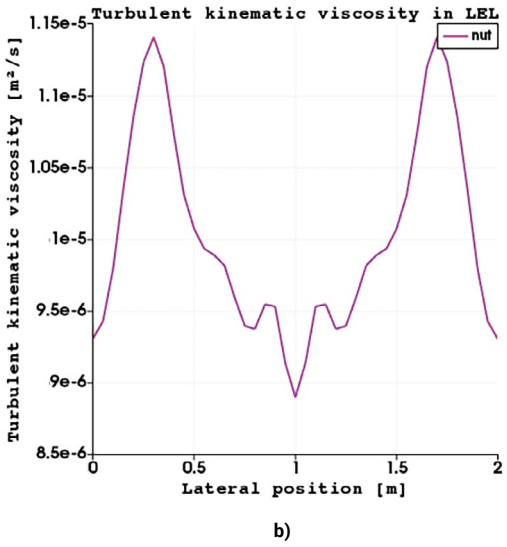


Figure 11. The kinematic turbulent viscosity v_t at a height of 0.05 *m* at 10 *s*: a) diagonal, b) lateral position

Source: Own elaboration.

The peaks in turbulent kinematic viscosity are distributed across three regions: the lowest values near the walls, the average values at approximately 0.5 m from the centre along the diagonal, and the highest value at the centre of the chamber, as shown in the graph on the left. In the graph on the right, which shows the values on the side walls, there are two peaks: the highest, of approximately $1.15e^{-5}m^2/s$, at 0.025 m from the corner, and the lowest, at the centre of the side wall, with a value of approximately $9e^{-6}m^2/s$. The effect of turbulent transport is therefore represented by nut, enabling the diffusion and redistribution of butane within the chamber to be interpreted.

Analysis of fields at the critical UEL point

Unlike the lower explosive limit, which was analysed using linear models at specific times and on specific surfaces within the chamber, the upper explosive limit is analysed using a time-dependent dynamic model. We examine the evolution of the 'UEL' at every instant throughout the 10-second simulation of butane gas dispersion within the kitchen chamber. The analysis is carried out using digital sensors within the chamber, the positions of which have been carefully selected. The gas container placed inside the chamber is initially filled to a volume of 0.672 m^3, representing 8.4% of the chamber's volume, as shown in [Figure 4]. When the gas is released, it gradually spreads throughout the chamber. Using the critical UEL value, the distribution of the gas within the enclosure can be analysed.

Table 2. Orientations of the four virtual sensors

Virtual sensor	Sensor 1	Sensor 2	Sensor 3	Sensor 4
Orientation [Figure 4]	Front	Right side	Left side	Bottom near the source

Source: Own elaboration.

The first three virtual sensors provided an opportunity to display simulation images and tables summarising, within 10 seconds, the effects occurring at each virtual sensor. However, for the fourth virtual sensor, the study focuses specifically on the area of the virtual sensor closest to the gas release in order to highlight certain key parameters of our modelling. To this end, particular emphasis is placed on the first 20-time steps, i.e. 1 s, corresponding to the first second. The position of the fourth virtual sensor is shown in pink in Figure 4. At this position, we can observe the behaviour of the fields right at the start when the gas is released; we are even able to obtain precise information on the turbulence at that exact moment.

Volume fraction and fluid velocity over time at virtual sensor 4 (UEL)

The two curves have been plotted on the same graph to observe how one varies with respect to the other. In Figure 12 below, the black graph shows the volume fraction and the blue graph shows the magnitude of the velocity at which the two fluids are moving within the chamber at this virtual sensor 4. This is a time series, and the focus will be in particular on what happens between 0 and 1 s.

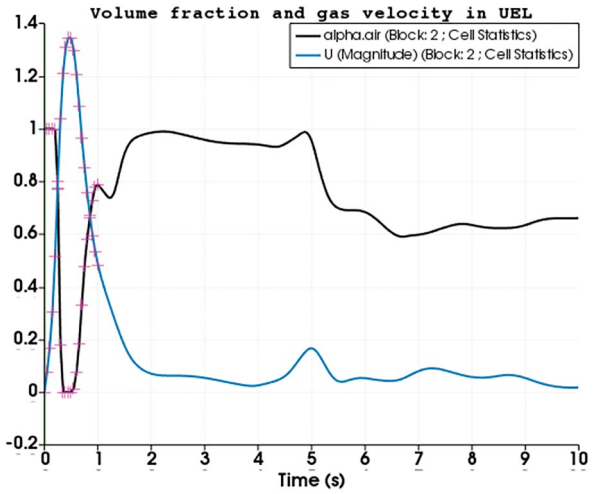


Figure 12. Temporal evolution of alpha.air the air/butane concentration [%] and U velocity [m/s] at virtual sensor 4 (UEL)

Source: Own elaboration.

The pink lines on the graphs mark the most significant area of the study at virtual sensor 4. There is a sharp increase in the gas propagation velocity once released; the velocity rises to approximately 1.35 m/s before reaching 0.5 s. The velocity then stabilises at values very close to between 0 and 0.1 m/s until the tenth second. Regarding the volume fraction of air and butane gas, we also observe very low air concentrations in this zone during the first few seconds, with air proportions dropping to near zero and leaving room only for the flow of butane gas, as at 0.4 s. This zone is particularly dominated by butane gas concentrations at the start, followed by a sort of return of air. Indeed, the air initially displaced by the butane gas gradually returns, and the mixing process continues as the experiment progresses until the tenth second, when the volume fraction of air stabilises between 0.5 and 0.6.

Combined fields v_t, k, ε over time at virtual sensor 4 (UEL)

In this section, the interpretation of the curves in the figure below reveals several details regarding the behaviour of the turbulent kinematic viscosity, turbulent kinetic energy and dissipation rate fields. The three curves reach their highest peaks between 0 and 2 seconds (see Figure 13).

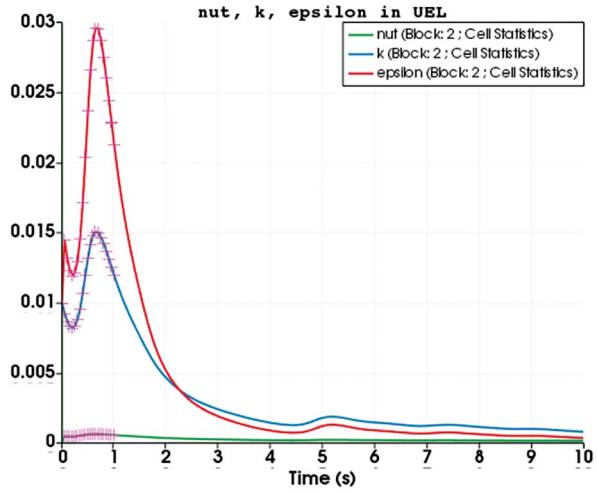


Figure 13. Temporal evolution of turbulent kinematic viscosity [m² · s⁻¹], k turbulent kinetic energy [m² · s⁻²], ε dissipation rate [m² · s⁻³] at virtual sensor 4 (UEL)

Source: Own elaboration.

After a second has elapsed, a gradual decrease in the field values is observed, leading to the gases stabilising within the closed chamber at this point. A proportional relationship is also observed between these three values; they evolve almost in unison, with values at around the tenth second being almost equal and all tending towards values very close to 0.

Static pressure and hydrostatic pressure at virtual sensor 4 (UEL)

The curves in the figure below show the static pressure and hydrostatic pressure at virtual sensor 4. The static pressure is represented by the purple curve and the hydrostatic pressure by the orange curve. The evolution of these curves provides information on the physical phenomena occurring at this level of the chamber from the first to the tenth second. For the 0.4 s time step, the diffusivities at virtual sensor 4 are:

$$v^4_{weig(0.4)} = 2.77 \times 10^{-6} m^2/s$$

$$D^{eff(4)}_{k(0.4)} = 7.88 \times 10^{-4} m^2/s$$

$$D^{eff(4)}_{\epsilon(0.4)} = 7.88 \times 10^{-4} m^2/s$$

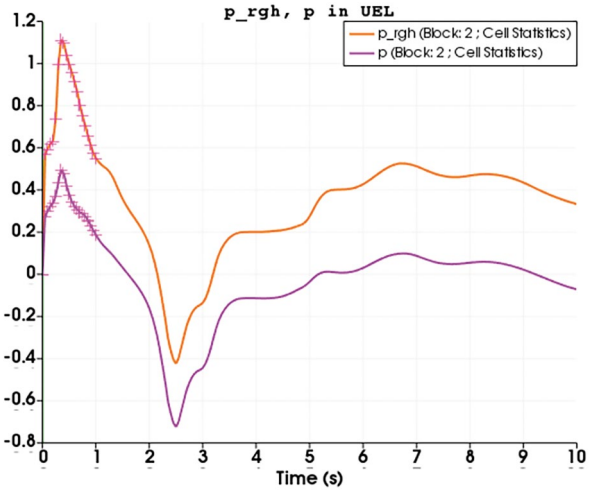


Figure 14. Temporal evolution of p static pressure (kinematic static pressure) [m² · s⁻²] and p_rgh hydrostatic pressure (pseudo-hydrostatic pressure) [Pa] at virtual sensor 4 (UEL). [p was obtained by division using a local ρ]

Source: Own elaboration.

The authors focus in particular on the time intervals between 0 and 1 second, and these sections have been marked with small pink lines on each curve. The curves have three distinct zones. The first zone is marked by a sudden rise in pressures, immediately followed by a rapid drop between the initial state and the first second, with peaks reaching approximately 0.5 m²/s² for static pressure and 1.1 Pa for hydrostatic pressure. Then, between the second and third seconds, these peaks drop further to approximately −0.7 m²/s² for static pressure and −0.4 Pa for hydrostatic pressure. This is followed by an increase in the values of these fields, fluctuating around 0 m²/s² for static pressure and 0.4 Pa for hydrostatic pressure between the third and tenth seconds (see Figure 14). Analysis of digital virtual sensor 4 regarding the Reynolds number [28] provides information on the level of turbulence in this part of the chamber. Three aspects of this turbulence are carefully examined: the molecular Reynolds number, the effective Reynolds number and the turbulent Reynolds number. However, the most significant Reynolds number is the effective Reynolds number, as it provides information on the combined effect of the molecular and turbulent components on the actual diffusion at that moment.

For this virtual sensor 4, at 0.4 s the Reynolds numbers are:

$$Re_{moll} = 23597.19$$
$$Re_{eff} = 115.42$$
$$Re_t = 2407.49$$

The position of these virtual sensors was also chosen on the basis of the phenomena observed during the simulation. The results show that, across the entire height of the walls under consideration, butane gas is more concentrated at a height of approximately 10 cm above the floor of the chamber, whilst the upper section, above 1 m, is entirely filled with air. These results indeed show that it is more effective to position cooking gas leak detection sensors closer to the floor in order to prevent or avoid certain explosion accidents [29], [30] such as the one that occurred in 2024 at a hotel training centre in Douala, leaving approximately 18 victims in its wake [4].

Conclusion

Throughout this study, which examined how to predict changes in the concentration of a combustible gas within an enclosed space and to determine the conditions under which its dispersion leads to the formation of a flammable atmosphere. The objective was to identify, within a confined space, the critical concentration zones for butane gas lying between the LEL and the UEL following a simulated leak of this gas. We chose kitchens as a case study due to the high number of accidents observed in these environments in recent years in Cameroon [4] and worldwide [2]. The model kitchen was first defined with dimensions of 2 × 2 × 2 m, and OpenFOAM simulation software was used to model and compute the various fields. The results reveal that the majority of critical gas concentrations are located in the lower regions of the chamber, approximately 10 cm above the floor. This work did not merely involve examining the concentration of the gas, but also establishing a relationship between its distribution and various flow-related fields. Despite the limitations of this study, which was confined to a small kitchen, the information derived from these results can provide a solid basis for fire safety engineers when designing kitchens [31], as well as for industries involved in the processing and storage of LPG, such as butane, to identify strategic locations for the installation of safety sensors and gas leak detectors for preventative purposes, in accordance with the specifications relating to the flammable properties of each gas. This work also provides a foundation for future large-scale CFD studies in kitchens concerning the risks of explosion associated with accidental gas leaks. Future work will consider incorporating an energy equation to simulate thermal convection in a kitchen and extend the simulation duration.

Table 3. Results at the various virtual sensors

	v_{weig} [m²/s]	$D_k^{eff}; D_\varepsilon^{eff}$ [m²/s]	Re_{mol}	Re_{eff}	Re_t
Sensor 1 (at t = 5 s)	$1.06 \cdot 10^{-5}$	$2.56 \cdot 10^{-4}$	1266.09	71.78	196.88
Sensor 2 (at t = 5 s)	$1.56 \cdot 10^{-5}$	$1.81 \cdot 10^{-4}$	10.66	1.23	90.58
Sensor 3 (at t = 5 s)	$1.51 \cdot 10^{-5}$	$3.01 \cdot 10^{-4}$	258.57	17.64	161.60
Sensor 4 (at t = 0.4 s)	$2.77 \cdot 10^{-5}$	$7.88 \cdot 10^{-4}$	23597.19	115.42	2407.59

Source: Own elaboration.

Symbols

dV – Volume element [m³]
U – Velocity [m · s⁻¹]
ρ – Density [kg · m⁻³]
t – Time [s]
T – Stress tensor [Pa]
f – Acceleration [m · s⁻²]
p – Static pressure (kinematic static pressure) [m² · s⁻²]
e_{tot} – Specific total energy [J · kg⁻¹]
q – Heat flux [W · m⁻²]
k – Turbulent kinetic energy [m² · s⁻²]
ε – Dissipation rate of turbulent kinetic energy [m² · s⁻³]
α_{air} (alpha.air) – Volume fraction of air [%]
α_{but} (alpha.butane) – Volume fraction of butane [%]
$p_{_rgh}$ – Hydrostatic pressure (pseudo-hydrostatic pressure) [Pa]
σ_k, σ_ε, C_1, C_2, C_3, C_μ, η_0, β – Model coefficients [-]
η – Correction factor constant [-]
D_k^{eff}, D_ε^{eff} – Effective diffusivities [m² · s⁻¹]
μ – Dynamic viscosity [kg · m⁻¹ ·s⁻¹]
v – Kinematic viscosity [m² · s⁻¹]
G – Generation of kinetic energy from turbulence due to buoyancy [W ·m⁻³]
S_{ij} – Deformation tensor [s⁻¹]
R_e – Reynolds number [-]
s – Specific energy source [W · kg⁻¹]
Re_{mol} – Molecular Reynolds number [-]
Re_t – Turbulent Reynolds number [-]
Re_{eff} – Effective Reynolds number [-]

Literature

[1] Onguene Mvogo P., Mouangue R., Tégawendé Zaida J., Obounou M., Ekobena Fouda H., *Building Fire: Experimental and Numerical Studies on Behaviour of Flows at Opening*, "J. Combust." 2019, 2019, 1–11, https://doi.org/10.1155/2019/2535073.

[2] Salem J., Smith A., *Manes M., Cooking Practices and Fires*, 2023.

[3] Yang K., Wu H., Chen Y., Pang L., *Effect of Room Layout on Natural Gas Explosion in Kitchen*, 2024, https://doi.org/10.21203/rs.3.rs-4404583/v1.

[4] Djene E., *Douala: 18 étudiants blessés dans l'explosion d'une bouteille de gaz*, "Actu Cameroun", https://actucameroun.com/2024/02/08/douala-18-etudiants-blesses-dans-lexplosion-dune-bouteille-de-gaz/ [accessed: 02.11.2025].

[5] Venetsanos A.G., Baraldi D., Adams P., Heggem P.S., Wilkening H., *CFD modelling of hydrogen release, dispersion and combustion for automotive scenarios*, "J. Loss Prev. Process Ind." 2008, 21, 2, 162–184, https://doi.org/10.1016/j.jlp.2007.06.016.

[6] Wang K., Wang Y., Xu C., Xu Z., Guo H., Xu J., *A new pressure--based gas diffusion coefficient model: Modeling, verification and analysis*, "J. Clean. Prod." 2025, 496, 144961, https://doi.org/10.1016/j.jclepro.2025.144961.

[7] Cariteau B., Brinster J., Tkatschenko I., *Experiments on the distribution of concentration due to buoyant gas low flow rate release in an enclosure*, "Int. J. Hydrogen Energy" 2011, 36, 3, 2505–2512, https://doi.org/10.1016/j.ijhydene.2010.04.054.

[8] De Stefano M., Rocourt X., Sochet I., Daudey N., *Hydrogen dispersion in a closed environment*, 2019.

[9] Safakar M., Syafiie S., Yunus R., *CFD Analysis of Indoor Chlorine Gas Dispersion Storage: Temperatures, Wind Velocities and Ventilation Effects Studies*, 2016, [online], https://journal.ugm.ac.id/AJChE/article/view/49669 [accessed: 05.07.2025].

[10] Moen A., Mauri L., Narasimhamurthy V., *Comparison of k-e models in gaseous release and dispersion simulations using the CFD code FLACS*, "Process Saf. Environ. Prot." 2019, 130, https://doi.org/10.1016/j.psep.2019.08.016.

[11] Middha P., Hansen O.R., Storvik I.E., *Validation of CFD--model for hydrogen dispersion*, "J. Loss Prev. Process Ind." 2009, 22, 6, 1034–1038, https://doi.org/10.1016/j.jlp.2009.07.020.

[12] Giannissi S.G. et al., *CFD benchmark on hydrogen release and dispersion in confined, naturally ventilated space with one vent*, "Int. J. Hydrogen Energy" 2015, 40, 2415–2429, https://doi.org/10.1016/j.ijhydene.2014.12.013.

[13] Prasad K., Pitts W.M., Yang J.C., *A Numerical Study Of The Release And Dispersion Of A Buoyant Gas In Partially Confined Spaces*, 2011, [online], https://tsapps.nist.gov/publication/get_pdf.cfm?pub_id=906120 [accessed: 05.07.2025].

[14] Bilyaz S., Ezekoye O.A., *Modeling the dispersion and mixing of light gases in enclosed spaces using the Method of Moments*, "J. Loss Prev. Process Ind." 2022, 80, 104877, https://doi.org/10.1016/j.jlp.2022.104877.

[15] Fiates J., Vianna S.S.V., *Numerical modelling of gas dispersion using OpenFOAM*, "Process Saf. Environ. Prot." 2016, 104, 277–293, https://doi.org/10.1016/j.psep.2016.09.011.

[16] Weller H.G., Tabor G., Jasak H., Fureby C., *A tensorial approach to computational continuum mechanics using object-oriented techniques*, "Comput. Phys." 1998, 12, 6, 620–631, https://doi.org/10.1063/1.168744.

[17] Greenshields C., *OpenFOAM v6 User Guide – Contents*, *OpenFOAM Foundation Ltd.*, [online], https://doc.cfd.direct/openfoam/user-guide-v6/contents [accessed: 16.07.2025].

[18] Petersen J.A., *National fire protection association standards in fire litigation*, "Eng. Stand. Forensic Appl." 2019, 155–168.

[19] Părăian M., Burian S., Vătavu N., Păun F., *Aspects regarding the applicability of ATEX directives for the evaluation of products regarding the risk of explosion*, "MATEC Web Conf." 2020, 305, 00009, https://doi.org/10.1051/matecconf/202030500009.

[20] Yakhot V., Orszag S.A., *Renormalization group analysis of turbulence. I. Basic theory*, "J. Sci. Comput." 1986, 1, 3–51.

[21] Dong L., Zuo H., Hu L., Yang B., Li L., Wu L., *Simulation of heavy gas dispersion in a large indoor space using CFD model*, "J. Loss Prev. Process Ind." 2017, 46, 1–12, https://doi.org/10.1016/j.jlp.2017.01.012.

[22] Hendiger J., Chludzińska M., Ziętek P., *Case Study of Dense Hazardous Gas Dispersion in Large Indoor Spaces: Ventilation Layout Analysis with Modeling*, "Sustainability" 2025, 17, 24, https://doi.org/10.3390/su172411367.

[23] Mack A., Spruijt M.P.N., *Validation of OpenFoam for heavy gas dispersion applications*, "J. Hazard. Mater." 2013, 262, 504–516, https://doi.org/10.1016/j.jhazmat.2013.08.065.

[24] Hirt C.W., Nichols B.D., *Volume of fluid (VOF) method for the dynamics of free boundaries*, "J. Comput. Phys." 1981, 39, 1, 201–225, https://doi.org/10.1016/0021-9991(81)90145-5.

[25] Wilcox D., *Turbulence Modeling for CFD* (Third Edition) (Hardcover), DCW Industries, La Canada CA, USA 2006.

[26] Meskéoulé Vondou F., Ngayihi Abbe C.V., Tégawendé Zaida J., Onguene Mvogo P., Mouangue R., *Experimental Study on Fire Behaviour in Room following the Disposition of Openings*, „Journal of Combustion" 2020, 2020, 9385712, 1–11, https://doi.org/10.1155/2020/9385712.

[27] Iya A.E.-k., Epée A.F., Mvogo P.O., Zaida J.T., Mouangue R., *Modelling and Numerical Simulation of a Compartment Fire: Flow Rate Behaviour at Opening*, „Fire" 2023, 6, 5, 185, https://doi.org/10.3390/fire6050185.

[28] White F.M., *Fluid Mechanics*, 7th ed., McGraw-Hill, New York 2011.

[29] Cyuzuzo T., Uwemeyimana Y., Emmanuel T., Niyonsaba J.L., Munyaneza C.U., Mwizerwa J.L., Rickard J., Debra R., Ntirenganya F., *Cooking Gas Explosion and Burn Accidents in Kigali: Epidemiological Profile and outcomes of patients admitted to the University Teaching Hospital of Kigali (CHUK)*, „East and Central African Journal of Surgery" 2025, 30, 2, 15–22, https://doi.org/10.4314/ecajs.v30i2.3.

[30] Codjoe A.B., Asare L.S., Tettey P., Ochieng C., Amegbor P., Boateng G., Sackey B., Addade M., Norvivor F.A., Quansah R., *Kitchen cooking burns: A real danger for adults and children in Ghana*, „Burns" 2025, 51, 4, 107458, https://doi.org/10.1016/j.burns.2025.107458.

[31] Institut National de Recherche et de Sécurité (INRS), *Conception des cuisines de restauration collective. Repères en hygiène et prévention des risques professionnels*, ED 6007, INRS, Paris 2007.

CÉDRIC TIAFOUDJI – is currently a monitor (teaching assistant) at the Energy Engineering Laboratory of the National Higher Polytechnic School of Douala (NHPSD), part of the University of Douala in Cameroon. His research focuses on fire safety and energy.

PHILIPPE ONGUENE MVOGO – is currently a lecturer at the School of Chemical Engineering and Mineral Industries (EGCIM) at the University of Ngaoundéré, Cameroon. His research focuses on combustion, bioclimatic comfort and fire safety.

FIDEL MESKÉOULÉ VONDOU – is currently a lecturer at the Faculty of Science, University of Garoua, Cameroon. His research focuses on combustion and industrial refrigeration.

EL-KEBIR IYA AHMED – is currently a lecturer at the National Higher Polytechnic School of Douala, part of the University of Douala in Cameroon. His research focuses on fire safety and bioenergy.

JUSTIN TÉGAWENDÉ ZAIDA – is currently a lecturer at the Higher Polytechnic School of Ouagadougou, Burkina Faso. His research focuses on combustion and pollution.

RUBEN MOUANGUE – is currently a lecturer and director at the National Higher Polytechnic School of Douala, part of the University of Douala, Cameroon. His research focuses on combustion and green energy.